

Multiuser MIMO-AFDM Beamforming for ISAC in Doubly Dispersive Channels

Rang Liu^{*}, Ming Li[†], A. Lee Swindlehurst[‡], Norman Franchi^{*}, and Robert Schober^{*}

^{*}Friedrich-Alexander-Universität Erlangen-Nürnberg (FAU), Erlangen 91058, Germany

[†]Dalian University of Technology, Dalian, Liaoning 116024, China

[‡]University of California, Irvine, CA 92697, USA

Email: rang.liu@fau.de, mli@dlut.edu.cn, swindle@uci.edu, {norman.franchi, robert.schober}@fau.de

Abstract—Integrated sensing and communication (ISAC) in high-mobility channels requires waveform and beamforming designs that are robust to delay-Doppler dispersion. With this in mind, in this paper we study a monostatic multiuser multiple-input multiple-output (MIMO) affine frequency division multiplexing (AFDM) downlink system. We develop a discrete affine Fourier transform (DAFT)-domain model that preserves Doppler-induced inter-bin coupling and derive a data-aided delay-Doppler detector. The expected matched-bin detector signal-to-noise ratio (SNR) is shown to be proportional to a transmit-covariance beampattern, which leads to a detector-SNR-based sector-illumination constraint. The resulting sensing-constrained weighted sum-rate maximization problem is solved using a combined weighted minimum mean squared error (WMMSE) and majorization-minimization (MM) formulation. Simulations show that the proposed AFDM design outperforms its orthogonal frequency division multiplexing (OFDM) counterpart in terms of the rate-sensing tradeoff, robustness to Doppler, and delay-Doppler sensing quality.

Index Terms—Integrated sensing and communication (ISAC), affine frequency division multiplexing (AFDM), multiuser MIMO, sensing-constrained beamforming, target detection.

I. INTRODUCTION

Orthogonal frequency division multiplexing (OFDM) has been widely adopted as a baseline waveform for integrated sensing and communication (ISAC), owing to its mature implementation and efficient time-frequency processing [1], [2]. However, in high-mobility wideband scenarios, doubly dispersive channels destroy subcarrier orthogonality, leading to Doppler-induced inter-carrier interference and delay-Doppler sensing leakage. Affine frequency division multiplexing (AFDM) has recently emerged as a promising alternative chirp-domain waveform for such channels [3]–[5]. By properly tuning its chirp parameters, AFDM provides a structured representation of delay-Doppler dispersion and improves robustness against rapidly varying sensing channels.

Recent AFDM-ISAC studies have focused on pilot-assisted delay-Doppler sensing, AFDM-parameter design, Cramér-Rao bound and ambiguity-function analysis, and transmit waveform optimization [6]–[9]. These studies have shown that properly designed AFDM pilots and parameters can improve delay-Doppler estimation, extend the unambiguous Doppler range, and provide useful insights into sensing accuracy and ambiguity behavior. However, most existing works focus on point-to-point AFDM-ISAC modeling, pilot-level sensing, receiver-side

estimation, or single-vector transmit waveform optimization, rather than multiuser multiple-input multiple-output (MIMO) downlink beamforming. A coherent processing interval (CPI)-level multiuser MIMO-AFDM ISAC framework that jointly addresses multiple data streams, Doppler-induced discrete affine Fourier transform (DAFT)-domain inter-bin coupling, block-level communication rates, data-aided target detection, and sensing-constrained beamforming is not available.

Motivated by this gap, this paper studies a monostatic multiuser MIMO-AFDM ISAC downlink system operating in doubly dispersive channels. We develop a CPI-level DAFT-domain communication and sensing model that retains off-grid Doppler-induced inter-bin coupling. For communication, we adopt a block-level achievable-rate metric for the coupled DAFT-domain symbols; for sensing, we derive a data-aided delay-Doppler matched-filter detector using the known AFDM waveform over the CPI, and show that its expected matched-bin detector signal-to-noise ratio (SNR) crucially depends on the transmit beampattern. This relationship leads to a detector-SNR-based sector-illumination constraint. We then formulate a sensing-constrained weighted sum-rate maximization problem and solve it using a combined weighted minimum mean squared error (WMMSE) and majorization-minimization (MM) formulation with convex quadratically constrained quadratic programming (QCQP) beamformer updates. Simulations demonstrate improved rate-sensing trade-offs, robustness to Doppler, and delay-Doppler sensing performance compared to OFDM.

Notation: The transpose, complex conjugate, and Hermitian transpose operations are denoted by $(\cdot)^T$, $(\cdot)^*$, and $(\cdot)^H$, respectively. The operators $\mathbb{E}\{\cdot\}$, $\text{tr}(\cdot)$, $\det(\cdot)$, $\text{vec}(\cdot)$, $\text{diag}\{\cdot\}$, and $\text{blkdiag}(\cdot)$ represent the expectation, trace, determinant, vectorization, diagonalization, and block-diagonalization functions, respectively. The fields of complex and real numbers are indicated by \mathbb{C} and \mathbb{R} , respectively. The circularly symmetric complex Gaussian distribution with mean vector $\boldsymbol{\mu}$ and covariance matrix \mathbf{C} is denoted by $\mathcal{CN}(\boldsymbol{\mu}, \mathbf{C})$. For Hermitian matrix \mathbf{X} , $\mathbf{X} \succ \mathbf{0}$ indicates that \mathbf{X} is positive definite. The $N \times N$ identity matrix is represented by \mathbf{I}_N .

II. MIMO-AFDM ISAC SYSTEM MODEL

We consider a monostatic AFDM-based ISAC downlink system, where an N_t -antenna base station (BS) serves K

single-antenna users and probes a point target. The BS is equipped with an N_r -element co-located receive uniform linear array (ULA) for monostatic sensing. Each transmitted block of AFDM data carries both information-bearing and dedicated sensing symbols, and the employed precoders must address multiuser communication and sensing requirements.

A. AFDM Transmit Signal Model

A given CPI consists of Q AFDM blocks indexed by $q \in \{0, \dots, Q-1\}$. Each AFDM block contains N affine-domain data/sensing symbols that are mapped to N time-domain samples spaced by the baseband sample interval T_s , and is preceded by a chirp-periodic prefix (CPP) of length N_{cpp} . The AFDM block duration is therefore $T_{\text{sym}} \triangleq (N + N_{\text{cpp}})T_s$. We assume $N_{\text{cpp}} \geq \ell_{\text{max}}$, where $\ell_{\text{max}}T_s$ denotes the maximum target delay considered in the system.

For DAFT bin $m \in \{0, \dots, N-1\}$ and AFDM block q , let $\mathbf{d}[m, q] \triangleq [d_1[m, q] \dots d_K[m, q]]^T \in \mathbb{C}^K$ denote the multiuser data symbol vector, and let $\mathbf{c}[m, q] \in \mathbb{C}^{L_s}$ denote the dedicated sensing-symbol vector, where L_s is the number of sensing streams. The data and sensing symbols are zero mean, unit variance, and mutually independent across signal streams, DAFT bins, and AFDM blocks. Hence, $\mathbb{E}\{\mathbf{d}[m, q]\mathbf{d}^H[m, q]\} = \mathbf{I}_K$ and $\mathbb{E}\{\mathbf{c}[m, q]\mathbf{c}^H[m, q]\} = \mathbf{I}_{L_s}$. The BS applies communication precoder $\mathbf{W}_c[m] \triangleq [\mathbf{w}_{c,1}[m], \dots, \mathbf{w}_{c,K}[m]] \in \mathbb{C}^{N_t \times K}$ and sensing precoder $\mathbf{W}_s[m] \in \mathbb{C}^{N_t \times L_s}$ for DAFT bin m . The precoders $\{\mathbf{W}_c[m], \mathbf{W}_s[m]\}_{m=0}^{N-1}$ are allowed to vary across DAFT bins but are kept fixed over one CPI. Thus, the DAFT-domain transmit vector across the N_t antennas is given by

$$\mathbf{s}[m, q] = \mathbf{W}_c[m]\mathbf{d}[m, q] + \mathbf{W}_s[m]\mathbf{c}[m, q] \in \mathbb{C}^{N_t \times 1}. \quad (1)$$

Stacking the DAFT-bin transmit vectors row-wise gives

$$\mathbf{S}[q] \triangleq [\mathbf{s}[0, q] \dots \mathbf{s}[N-1, q]]^T \in \mathbb{C}^{N \times N_t}. \quad (2)$$

The time-domain AFDM block is generated by applying the inverse DAFT to each transmit-antenna column, i.e.,

$$\mathbf{X}[q] \triangleq \mathbf{A}^H \mathbf{S}[q] \in \mathbb{C}^{N \times N_t}, \quad (3)$$

where $\mathbf{A} \triangleq \mathbf{\Lambda}_{c_2} \mathbf{F} \mathbf{\Lambda}_{c_1} \in \mathbb{C}^{N \times N}$ is the unitary DAFT matrix, $\mathbf{F} \in \mathbb{C}^{N \times N}$ is the normalized discrete Fourier transform (DFT) matrix, and

$$\mathbf{\Lambda}_{c_1} \triangleq \text{diag}\{e^{-j2\pi c_1 n^2}\}_{n=0}^{N-1}, \quad \mathbf{\Lambda}_{c_2} \triangleq \text{diag}\{e^{-j2\pi c_2 m^2}\}_{m=0}^{N-1}.$$

Chirp parameters c_1 and c_2 are chosen according to the delay-Doppler support of the channel. If $c_1 = c_2 = 0$, the model reduces to block-processed OFDM, the CPP becomes the conventional cyclic prefix, and \mathbf{A} the normalized DFT matrix.

B. Doubly Dispersive MIMO Channel Model

Here we derive a generic DAFT-domain representation for a far-field, spatially narrowband, doubly dispersive MIMO channel. For a ULA with half-wavelength spacing, the transmit steering vector for angle θ is $\mathbf{a}_t(\theta) \triangleq [1 e^{-j\pi \sin(\theta)} \dots e^{-j(N_t-1)\pi \sin(\theta)}]^T \in \mathbb{C}^{N_t}$, and the receive

steering vector $\mathbf{a}_r(\theta) \in \mathbb{C}^{N_r}$ is defined analogously. Let $\alpha_p \in \mathbb{C}$, $\tau_p \in \mathbb{R}$, and $f_p \in \mathbb{R}$ denote the complex gain, propagation delay, and Doppler shift of channel path p , respectively. The corresponding angle of departure (AoD) and angle of arrival (AoA) are denoted by $\theta_{t,p}$ and $\theta_{r,p}$, respectively. The spatial signature of path p is

$$\Theta_p \triangleq \mathbf{a}_r(\theta_{r,p})\mathbf{a}_t^H(\theta_{t,p}) \in \mathbb{C}^{N_r \times N_t}. \quad (4)$$

For monostatic sensing, the transmit and receive angles coincide, i.e., $\theta_{t,p} = \theta_{r,p} = \theta_p$. For a single-antenna user, the receive-side array response reduces to a scalar and is absorbed into the path gain. The path delays are represented by sample-spaced taps of the discrete-time equivalent channel after synchronization and sampling, i.e., $\tau_p = \ell_p T_s$ with $\ell_p \in \{0, \dots, \ell_{\text{max}}\}$. This approximation is reasonable for the considered wideband setting, where the sampling interval provides a fine delay grid [3]. In contrast, the Doppler shifts $f_p \in \mathbb{R}$ are retained as continuous physical parameters and are not restricted to the Doppler grid. The continuous-time, time-varying impulse response between transmit antenna n_t and receive antenna n_r is modeled as

$$h_{n_r, n_t}(t, \tau) = \sum_{p=1}^{P_g} \alpha_p e^{j2\pi f_p t} [\Theta_p]_{n_r, n_t} \delta(\tau - \tau_p), \quad (5)$$

where P_g denotes the number of paths.

After sampling and CPP removal, the sample-spaced delay model preserves the CPP-induced chirp-circular shift structure. Specifically, the integer delay $\ell \leq N_{\text{cpp}}$ is represented by the chirp-circular operator $\Psi(\ell) \triangleq \Gamma_{\text{CPP}}(\ell)\mathbf{\Pi}^\ell$, where $\mathbf{\Pi}$ is the cyclic-shift matrix and $\Gamma_{\text{CPP}}(\ell)$ is the unitary diagonal CPP phase-correction matrix for AFDM [4]. In AFDM block q , the Doppler phase can be decomposed into a slow-time phase across AFDM blocks and a fast-time modulation within each block: $e^{j2\pi f(qT_{\text{sym}} + nT_s)} = b_q(f)e^{j2\pi f nT_s}$, where

$$b_q(f) \triangleq e^{j2\pi f q T_{\text{sym}}}, \quad q = 0, \dots, Q-1, \quad (6a)$$

$$\Delta(f) \triangleq \text{diag}\{e^{j2\pi f nT_s}\}_{n=0}^{N-1} \in \mathbb{C}^{N \times N}. \quad (6b)$$

Thus, the time-domain delay-Doppler operator for one path is

$$\mathbf{T}(\ell, f) \triangleq \Delta(f)\Psi(\ell) \in \mathbb{C}^{N \times N}. \quad (7)$$

Let $\tilde{\mathbf{Y}}_g[q] \in \mathbb{C}^{N \times N_r}$ denote the received time-domain data block after CPP removal. Combining the temporal delay-Doppler operator and the channel's spatial response yields

$$\tilde{\mathbf{Y}}_g[q] = \sum_{p=1}^{P_g} \alpha_p b_q(f_p) \mathbf{T}(\ell_p, f_p) \mathbf{X}[q] \Theta_p^T + \tilde{\mathbf{N}}_g[q], \quad (8)$$

where $\mathbf{X}[q] \in \mathbb{C}^{N \times N_t}$ is the block of time-domain transmit data and $\tilde{\mathbf{N}}_g[q]$ is noise. Applying the DAFT to each receive-antenna column and using $\mathbf{X}[q] = \mathbf{A}^H \mathbf{S}[q]$, we obtain

$$\mathbf{Y}_g[q] = \mathbf{A} \tilde{\mathbf{Y}}_g[q] \quad (9a)$$

$$= \sum_{p=1}^{P_g} \alpha_p b_q(f_p) \mathbf{A} \mathbf{T}(\ell_p, f_p) \mathbf{A}^H \mathbf{S}[q] \Theta_p^T + \mathbf{N}_g[q], \quad (9b)$$

where $\mathbf{N}_g[q] \triangleq \mathbf{A}\tilde{\mathbf{N}}_g[q]$. If $\tilde{\mathbf{N}}_g[q]$ has independent and identically distributed (i.i.d.) $\mathcal{CN}(0, \sigma^2)$ entries, then so will $\mathbf{N}_g[q]$ due to the unitarity of \mathbf{A} . The corresponding DAFT-domain delay-Doppler operator is therefore defined as

$$\mathbf{E}(\ell, f) \triangleq \mathbf{A}\mathbf{T}(\ell, f)\mathbf{A}^H = \mathbf{A}\mathbf{\Delta}(f)\mathbf{\Psi}(\ell)\mathbf{A}^H \in \mathbb{C}^{N \times N}. \quad (10)$$

Since \mathbf{A} , $\mathbf{\Delta}(f)$, and $\mathbf{\Psi}(\ell)$ are unitary, $\mathbf{E}(\ell, f)$ is also unitary. Thus, the corresponding generic DAFT-domain MIMO input-output relationship is given by

$$\mathbf{Y}_g[q] = \sum_{p=1}^{P_g} \alpha_p b_q(f_p) \mathbf{E}(\ell_p, f_p) \mathbf{S}[q] \mathbf{\Theta}_p^T + \mathbf{N}_g[q]. \quad (11)$$

Note that (11) retains the full DAFT-domain delay-Doppler operator $\mathbf{E}(\ell_p, f_p)$, thereby capturing the inter-bin coupling induced by off-grid Doppler shifts. The downlink communication and monostatic sensing models used below follow as special cases of this generic model.

C. Multiuser Communication Model and Performance Metric

We now adapt (11) to the multiuser downlink with single-antenna users, where the channel of user k comprises P_k paths parameterized by $\{\alpha_{k,p}, \ell_{k,p}, f_{k,p}, \theta_{k,p}\}_{p=1}^{P_k}$. The received DAFT-domain block at user k during AFDM block q is then given by

$$\mathbf{z}_k[q] = \sum_{p=1}^{P_k} \alpha_{k,p} b_q(f_{k,p}) \mathbf{E}(\ell_{k,p}, f_{k,p}) \mathbf{S}[q] \mathbf{a}_t^*(\theta_{k,p}) + \mathbf{v}_k[q], \quad (12)$$

where $\mathbf{v}_k[q] \sim \mathcal{CN}(0, \sigma_c^2 \mathbf{I}_N)$ denotes white Gaussian noise at user k .

For the subsequent beamforming design, we collect the DAFT-bin symbols and precoders of one AFDM block. Define the stacked user-data vector $\bar{\mathbf{d}}_k[q] \triangleq [d_k[0, q] \cdots d_k[N-1, q]]^T \in \mathbb{C}^N$, and the stacked sensing-symbol vector $\bar{\mathbf{c}}[q] \triangleq [\mathbf{c}^T[0, q] \cdots \mathbf{c}^T[N-1, q]]^T \in \mathbb{C}^{NL_s}$. The corresponding block-diagonal communication and sensing precoders are given by

$$\bar{\mathbf{W}}_{c,k} \triangleq \text{blkdiag}(\mathbf{w}_{c,k}[0], \dots, \mathbf{w}_{c,k}[N-1]) \in \mathbb{C}^{NN_t \times N}, \quad (13)$$

$$\bar{\mathbf{W}}_s \triangleq \text{blkdiag}(\mathbf{W}_s[0], \dots, \mathbf{W}_s[N-1]) \in \mathbb{C}^{NN_t \times NL_s}. \quad (14)$$

Using $\bar{\mathbf{s}}[q] \triangleq \text{vec}(\mathbf{S}^T[q])$, the stacked transmit vector can be written as

$$\bar{\mathbf{s}}[q] = \sum_{j=1}^K \bar{\mathbf{W}}_{c,j} \bar{\mathbf{d}}_j[q] + \bar{\mathbf{W}}_s \bar{\mathbf{c}}[q] \in \mathbb{C}^{NN_t \times 1}. \quad (15)$$

By construction, the m -th N_t -dimensional block of $\bar{\mathbf{s}}[q]$ corresponds to the DAFT-bin transmit vector $\mathbf{s}[m, q]$. For path p of user k , define the angular projection matrix $\mathbf{\Phi}_{k,p} \triangleq \mathbf{I}_N \otimes \mathbf{a}_t^H(\theta_{k,p}) \in \mathbb{C}^{N \times NN_t}$, which satisfies $\mathbf{\Phi}_{k,p} \bar{\mathbf{s}}[q] = \mathbf{S}[q] \mathbf{a}_t^*(\theta_{k,p})$. The effective DAFT-domain channel of user k in block q is then given by

$$\mathbf{H}_k[q] \triangleq \sum_{p=1}^{P_k} \alpha_{k,p} b_q(f_{k,p}) \mathbf{E}(\ell_{k,p}, f_{k,p}) \mathbf{\Phi}_{k,p} \in \mathbb{C}^{N \times NN_t}. \quad (16)$$

Thus, (12) can be compactly rewritten as

$$\mathbf{z}_k[q] = \sum_{j=1}^K \mathbf{H}_k[q] \bar{\mathbf{W}}_{c,j} \bar{\mathbf{d}}_j[q] + \mathbf{H}_k[q] \bar{\mathbf{W}}_s \bar{\mathbf{c}}[q] + \mathbf{v}_k[q]. \quad (17)$$

Because off-grid Doppler generally makes $\mathbf{E}(\ell_{k,p}, f_{k,p})$ dense in the DAFT domain, the effective channel $\mathbf{H}_k[q]$ couples the N DAFT bins. A per-bin signal-to-interference-plus-noise (SINR) problem formulation is therefore not appropriate. We instead adopt a block information-rate metric over the N coupled DAFT-domain symbols. The interference-plus-noise covariance of user k in block q is given by

$$\begin{aligned} \Sigma_k[q] &\triangleq \sum_{j \neq k} \mathbf{H}_k[q] \bar{\mathbf{W}}_{c,j} \bar{\mathbf{W}}_{c,j}^H \mathbf{H}_k^H[q] \\ &\quad + \mathbf{H}_k[q] \bar{\mathbf{W}}_s \bar{\mathbf{W}}_s^H \mathbf{H}_k^H[q] + \sigma_c^2 \mathbf{I}_N. \end{aligned} \quad (18)$$

Assuming Gaussian signaling and joint decoding over the N coupled DAFT-domain symbols, the achievable block rate of user k is given by

$$R_k[q] = \log_2 \det(\mathbf{I}_N + \Sigma_k^{-1}[q] \mathbf{H}_k[q] \bar{\mathbf{W}}_{c,k} \bar{\mathbf{W}}_{c,k}^H \mathbf{H}_k^H[q]). \quad (19)$$

The CPI-averaged achievable block rate is then defined as

$$\bar{R}_k \triangleq \frac{1}{Q} \sum_{q=0}^{Q-1} R_k[q], \quad (20)$$

which serves as the communication metric for the proposed sensing-constrained beamforming design.

III. AFDM TARGET DETECTION AND SENSING METRIC

This section develops the receiver-side signal processing for monostatic AFDM target detection and derives a detection-SNR metric for transmit beamforming design. Leveraging the known AFDM transmit blocks, the monostatic receiver constructs a data-aided delay-Doppler statistic, whose matched-bin SNR quantifies target detectability. We further show that the expected detector SNR is proportional to the transmit-covariance beampattern, motivating the sensing constraint adopted for beamforming design in Section IV.

A. Data-Aided Delay-Doppler Matched Filtering

Consider a point target characterized by $\{\alpha, \theta, \ell, f\}$, where $\alpha \in \mathbb{C}$ is the complex reflection coefficient, θ is the target angle, ℓ is the on-grid delay, and $f \in \mathbb{R}$ is the Doppler shift. Since the transmitter and receiver are co-located, the AoD and AoA coincide, and the monostatic spatial response is $\mathbf{\Theta}(\theta) \triangleq \mathbf{a}_r(\theta) \mathbf{a}_t^H(\theta) \in \mathbb{C}^{N_r \times N_t}$. From (11), the received DAFT-domain reflection from a single target is given by

$$\mathbf{Y}[q] = \alpha b_q(f) \mathbf{E}(\ell, f) \mathbf{S}[q] \mathbf{\Theta}^T(\theta) + \mathbf{N}_s[q], \quad (21)$$

where $\mathbf{N}_s[q]$ has i.i.d. $\mathcal{CN}(0, \sigma_s^2)$ entries. Since the transmitted block $\mathbf{S}[q]$ is known at the monostatic receiver, it can be used for data-aided matched filtering over candidate delay-Doppler bins. For a delay-Doppler hypothesis (ℓ', ν) , where

$\ell' \in \{0, \dots, \ell_{\max}\}$, and $\nu \in \Omega_\nu$ for sampled Doppler search grid Ω_ν , the monostatic receiver forms

$$\bar{\mathbf{Z}}[\ell', \nu] = \sum_{q=0}^{Q-1} b_q^*(\nu) \mathbf{S}^H[q] \mathbf{E}^H(\ell', \nu) \mathbf{Y}[q] \in \mathbb{C}^{N_t \times N_r}. \quad (22)$$

In (22), $\mathbf{E}^H(\ell', \nu)$ compensates for the hypothesized DAFT-domain delay-Doppler response, $\mathbf{S}^H[q]$ performs known-waveform matched filtering, and $b_q^*(\nu)$ aligns the slow-time Doppler phase before coherent integration across the Q AFDM blocks. Thus, $\bar{\mathbf{Z}}[\ell', \nu]$ is the virtual MIMO observation associated with the hypothesized delay-Doppler bin.

Define $\mathbf{z}[\ell', \nu] \triangleq \text{vec}(\bar{\mathbf{Z}}[\ell', \nu]) \in \mathbb{C}^{N_t N_r \times 1}$ and the virtual steering vector $\mathbf{a}_v(\theta) \triangleq \text{vec}(\boldsymbol{\Theta}^T(\theta)) = \mathbf{a}_r(\theta) \otimes \mathbf{a}_t^*(\theta)$. Substituting (21) into (22) gives the matched-filter output at a generic delay-Doppler bin as

$$\mathbf{z}[\ell', \nu] = \alpha (\mathbf{I}_{N_r} \otimes \boldsymbol{\Xi}[\ell', \nu]) \mathbf{a}_v(\theta) + \mathbf{z}_n[\ell', \nu], \quad (23)$$

where

$$\boldsymbol{\Xi}[\ell', \nu] \triangleq \sum_{q=0}^{Q-1} b_q^*(\nu) b_q(f) \mathbf{S}^H[q] \mathbf{E}^H(\ell', \nu) \mathbf{E}(\ell, f) \mathbf{S}[q] \quad (24)$$

is the waveform correlation matrix between the hypothesized and true delay-Doppler responses, and

$$\mathbf{z}_n[\ell', \nu] = \text{vec} \left(\sum_{q=0}^{Q-1} b_q^*(\nu) \mathbf{S}^H[q] \mathbf{E}^H(\ell', \nu) \mathbf{N}_s[q] \right) \quad (25)$$

is the noise term. Conditioned on the transmitted blocks $\{\mathbf{S}[q]\}_{q=0}^{Q-1}$, the covariance of $\mathbf{z}_n[\ell', \nu]$ is obtained as

$$\mathbf{R}_n \triangleq \mathbb{E} \left\{ \mathbf{z}_n[\ell', \nu] \mathbf{z}_n^H[\ell', \nu] \mid \{\mathbf{S}[q]\}_{q=0}^{Q-1} \right\} = \sigma_s^2 (\mathbf{I}_{N_r} \otimes \mathbf{G}), \quad (26)$$

where we define

$$\mathbf{G} \triangleq \sum_{q=0}^{Q-1} \mathbf{S}^H[q] \mathbf{S}[q]. \quad (27)$$

The matched-filter output in (23) provides one virtual MIMO observation for each delay-Doppler hypothesis. Since the front-end search is performed over the delay-Doppler grid only, the target angle is not introduced as an additional search dimension in the sensing map. Instead, it remains in the virtual steering vector $\mathbf{a}_v(\theta)$ and determines the strength of the signal component associated with each delay-Doppler bin.

B. Detector SNR and Sensing Constraint

The matched-filter outputs in (23) are converted to a delay-Doppler sensing map through the whitened energy statistic:

$$T_{\text{DD}}(\ell', \nu) = \mathbf{z}^H[\ell', \nu] (\mathbf{R}_n + \epsilon \mathbf{I}_{N_t N_r})^{-1} \mathbf{z}[\ell', \nu], \quad (28)$$

where $\epsilon \geq 0$ is a diagonal-loading factor for numerical regularization. A candidate delay-Doppler bin is declared occupied when $T_{\text{DD}}(\ell', \nu) \geq \eta_{\text{FA}}$, where η_{FA} is selected according to the desired false-alarm probability.

We use the matched-bin detector SNR to quantify target detectability. For a matched delay-Doppler hypothesis, i.e.,

$(\ell', \nu) = (\ell, f)$, we have $\boldsymbol{\Xi}[\ell, f] = \mathbf{G}$, and (23) reduces to

$$\mathbf{z}[\ell, f] = \alpha (\mathbf{I}_{N_r} \otimes \mathbf{G}) \mathbf{a}_v(\theta) + \mathbf{z}_n[\ell, f]. \quad (29)$$

For ideal whitening with $\epsilon = 0$ and $\mathbf{R}_n \succ 0$, the squared norm of the whitened target component, i.e., the noncentrality parameter of the ideal whitened energy detector and the conditional matched-bin detector SNR, is given by

$$\lambda_{\text{DD}}(\theta) = |\alpha|^2 \mathbf{a}_v(\theta)^H (\mathbf{I}_{N_r} \otimes \mathbf{G})^H \mathbf{R}_n^{-1} (\mathbf{I}_{N_r} \otimes \mathbf{G}) \mathbf{a}_v(\theta) \quad (30a)$$

$$= N_r |\alpha|^2 \sigma_s^{-2} \mathbf{a}_t^H(\theta) \mathbf{G} \mathbf{a}_t(\theta), \quad (30b)$$

where $\mathbf{R}_n = \sigma_s^2 (\mathbf{I}_{N_r} \otimes \mathbf{G})$ and $\mathbf{a}_v(\theta) = \mathbf{a}_r(\theta) \otimes \mathbf{a}_t^*(\theta)$. For a fixed false-alarm probability, the detection probability is monotone in $\lambda_{\text{DD}}(\theta)$.

The instantaneous SNR in (30b) depends on the data-aided waveform through \mathbf{G} . Since the beamformers are fixed over the CPI whereas the transmitted data and sensing symbols are random, we use the ensemble-averaged matched-bin SNR as a deterministic beamforming metric. From the independence and unit variance of the transmitted symbols, we have

$$\mathbb{E}\{\mathbf{G}\} = Q \mathbf{R}_x^*, \quad (31)$$

where

$$\mathbf{R}_x \triangleq \sum_{m=0}^{N-1} \left(\sum_{k=1}^K \mathbf{w}_{c,k}[m] \mathbf{w}_{c,k}^H[m] + \mathbf{W}_s[m] \mathbf{W}_s^H[m] \right) \quad (32)$$

is the aggregated transmit covariance over the DAFT bins. Since \mathbf{R}_x is Hermitian, taking the expectation of (30b) yields

$$\mathbb{E}\{\lambda_{\text{DD}}(\theta)\} = N_r Q |\alpha|^2 \sigma_s^{-2} \mathbf{a}_t^H(\theta) \mathbf{R}_x \mathbf{a}_t(\theta). \quad (33)$$

Thus, the beamformer-dependent part of the expected target-bin detector SNR is the transmit-covariance beampattern $p_{\text{sen}}(\theta) \triangleq \mathbf{a}_t^H(\theta) \mathbf{R}_x \mathbf{a}_t(\theta)$. As the target direction is only known to lie in the sensing sector Θ_{sen} , we impose the detector-SNR requirement over a sampled angular grid $\mathcal{G} = \{\theta_1, \dots, \theta_{N_\theta}\} \subset \Theta_{\text{sen}}$:

$$p_{\text{sen}}(\theta_i) = \mathbf{a}_t^H(\theta_i) \mathbf{R}_x \mathbf{a}_t(\theta_i) \geq \Gamma_s, \quad i = 1, \dots, N_\theta. \quad (34)$$

Equivalently, this constraint ensures that the ensemble-averaged target-bin detector SNR is lower bounded in each sampled direction θ_i by $\gamma_{\text{req}} = N_r Q |\alpha|^2 \Gamma_s \sigma_s^{-2}$.

IV. SENSING-CONSTRAINED BEAMFORMING DESIGN

A. Problem Formulation

Under the detection-SNR-based sensing constraint derived in Section III, we jointly optimize the communication and sensing beamformers to maximize the weighted sum rate:

$$\max_{\mathcal{W}} \sum_{k=1}^K \mu_k \bar{R}_k(\mathcal{W}) \quad (35a)$$

$$\text{s.t. } \mathbf{a}_t^H(\theta_i) \mathbf{R}_x(\mathcal{W}) \mathbf{a}_t(\theta_i) \geq \Gamma_s, \quad i = 1, \dots, N_\theta, \quad (35b)$$

$$\text{tr}(\mathbf{R}_x(\mathcal{W})) \leq P_{\text{max}}, \quad (35c)$$

where $\mathcal{W} \triangleq \{\mathbf{w}_{c,k}[m], \mathbf{w}_{s,\ell_s}[m], \forall k, \ell_s, m\}$ collects all beam vectors, and $\mathbf{w}_{s,\ell_s}[m]$ denotes the ℓ_s -th column of $\mathbf{W}_s[m]$.

The covariance $\mathbf{R}_x(\mathcal{W})$ is given in (32), $\bar{R}_k(\mathcal{W})$ is the CPI-averaged rate of user k , and $\mu_k \geq 0$ is its weight. Constraint (35b) enforces the required sensing illumination power level Γ_s , while (35c) imposes the total transmit-power budget P_{\max} . Problem (35) is non-convex because the user rates are coupled by multiuser interference and the sensing constraints are super-level quadratic constraints.

B. WMMSE-MM Beamformer Optimization

We solve (35) by combining a WMMSE reformulation of the weighted sum rate objective function and an MM inner approximation of the non-convex sensing constraints.

1) *WMMSE-based Transformation*: We first rewrite the communication objective in a WMMSE form. For user k in AFDM block q , define the total receive covariance matrix

$$\mathbf{C}_k[q] \triangleq \boldsymbol{\Sigma}_k[q] + \mathbf{H}_k[q] \overline{\mathbf{W}}_{c,k} \overline{\mathbf{W}}_{c,k}^H \mathbf{H}_k^H[q], \quad (36)$$

which includes the desired signal, multiuser interference, dedicated sensing streams, and noise. For a linear receiver $\mathbf{U}_k[q] \in \mathbb{C}^{N \times N}$, the MSE matrix for estimating the desired DAFT-domain symbol vector of user k is

$$\mathbf{E}_k[q] = \mathbf{U}_k^H[q] \mathbf{C}_k[q] \mathbf{U}_k[q] - \mathbf{U}_k^H[q] \mathbf{H}_k[q] \overline{\mathbf{W}}_{c,k} - \overline{\mathbf{W}}_{c,k}^H \mathbf{H}_k^H[q] \mathbf{U}_k[q] + \mathbf{I}_N. \quad (37)$$

By further introducing a positive definite weighting matrix $\mathbf{M}_k[q] \succ \mathbf{0}$ and using $-\ln \det(\mathbf{E}) = \max_{\mathbf{M} \succ \mathbf{0}} \{\ln \det(\mathbf{M}) - \text{tr}(\mathbf{M}\mathbf{E}) + N\}$ [10], the block rate is equivalently written as

$$R_k[q] = \max_{\mathbf{U}_k[q], \mathbf{M}_k[q] \succ \mathbf{0}} \frac{1}{\ln 2} \left[\ln \det(\mathbf{M}_k[q]) - \text{tr}(\mathbf{M}_k[q] \mathbf{E}_k[q]) + N \right]. \quad (38)$$

Since the constraints involve only \mathcal{W} , the auxiliary variables can be updated in closed form at a feasible reference point \mathcal{W}^{ref} :

$$\mathbf{U}_k[q] = (\mathbf{C}_k^{\text{ref}}[q])^{-1} \mathbf{H}_k[q] \overline{\mathbf{W}}_{c,k}^{\text{ref}}, \quad (39a)$$

$$\mathbf{E}_k^{\text{ref}}[q] = \mathbf{I}_N - (\overline{\mathbf{W}}_{c,k}^{\text{ref}})^H \mathbf{H}_k^H[q] \mathbf{U}_k[q], \quad (39b)$$

$$\mathbf{M}_k[q] = (\mathbf{E}_k^{\text{ref}}[q])^{-1}, \quad (39c)$$

where \mathcal{W}^{ref} contains the feasible beamformers available at the beginning of the update and all quantities with superscript “ref” are evaluated using \mathcal{W}^{ref} .

For fixed auxiliary variables, maximizing the WMMSE surrogate over \mathcal{W} is equivalent to minimizing

$$\sum_{k=1}^K \frac{\mu_k}{Q \ln 2} \sum_{q=0}^{Q-1} \text{tr}(\mathbf{M}_k[q] \mathbf{E}_k[q]), \quad (40)$$

where $\mathbf{E}_k[q]$ is obtained with (37) using the candidate beamformers \mathcal{W} and the fixed receive filter $\mathbf{U}_k[q]$. Expanding (40) and dropping constants independent of \mathcal{W} gives a convex quadratic objective:

$$f_{\text{WMMSE}}(\mathcal{W}; \mathcal{W}^{\text{ref}}) = \sum_{j=1}^K \text{tr}(\overline{\mathbf{W}}_{c,j}^H \mathbf{T}_w \overline{\mathbf{W}}_{c,j})$$

$$+ \text{tr}(\overline{\mathbf{W}}_s^H \mathbf{T}_w \overline{\mathbf{W}}_s) - 2 \sum_{k=1}^K \Re \{ \text{tr}(\mathbf{B}_k^H \overline{\mathbf{W}}_{c,k}) \}, \quad (41)$$

where

$$\mathbf{T}_w \triangleq \sum_{k=1}^K \frac{\mu_k}{Q \ln 2} \sum_{q=0}^{Q-1} \mathbf{H}_k^H[q] \mathbf{U}_k[q] \mathbf{M}_k[q] \mathbf{U}_k^H[q] \mathbf{H}_k[q], \quad (42a)$$

$$\mathbf{B}_k \triangleq \frac{\mu_k}{Q \ln 2} \sum_{q=0}^{Q-1} \mathbf{H}_k^H[q] \mathbf{U}_k[q] \mathbf{M}_k[q]. \quad (42b)$$

2) *MM-based Transformation*: We next minorize the non-convex sensing constraints. Let $\mathbf{a}_i \triangleq \mathbf{a}_t(\theta_i)$ and rewrite the transmit beampattern as

$$g_i(\mathcal{W}) \triangleq \mathbf{a}_i^H \mathbf{R}_x(\mathcal{W}) \mathbf{a}_i = \sum_{\mathbf{w} \in \mathcal{W}} |\mathbf{a}_i^H \mathbf{w}|^2. \quad (43)$$

Although $g_i(\mathcal{W})$ is a convex quadratic in the beam vectors, the constraint $g_i(\mathcal{W}) \geq \Gamma_s$ is non-convex. For each $\mathbf{w} \in \mathcal{W}$ with corresponding reference vector \mathbf{w}^{ref} , the first-order lower bound of $|\mathbf{a}_i^H \mathbf{w}|^2$ is given by

$$|\mathbf{a}_i^H \mathbf{w}|^2 \geq 2 \Re \{ \mathbf{w}^H \mathbf{a}_i \mathbf{a}_i^H \mathbf{w}^{\text{ref}} \} - |\mathbf{a}_i^H \mathbf{w}^{\text{ref}}|^2. \quad (44)$$

Applying this bound to all beam vectors yields the affine minorant:

$$\tilde{g}_i(\mathcal{W}; \mathcal{W}^{\text{ref}}) = \sum_{\mathbf{w} \in \mathcal{W}} [2 \Re \{ \mathbf{w}^H \mathbf{a}_i \mathbf{a}_i^H \mathbf{w}^{\text{ref}} \} - |\mathbf{a}_i^H \mathbf{w}^{\text{ref}}|^2]. \quad (45)$$

This minorant is tight at \mathcal{W}^{ref} and satisfies $g_i(\mathcal{W}) \geq \tilde{g}_i(\mathcal{W}; \mathcal{W}^{\text{ref}})$, thus enforcing $\tilde{g}_i(\mathcal{W}; \mathcal{W}^{\text{ref}}) \geq \Gamma_s$ yields an inner approximation of the original sensing constraint.

3) *Beamformer Update*: Combining the WMMSE objective and the lower-bounded sensing constraints, the beamformer update is obtained by solving

$$\min_{\mathcal{W}} f_{\text{WMMSE}}(\mathcal{W}; \mathcal{W}^{\text{ref}}) \quad (46a)$$

$$\text{s.t. } \tilde{g}_i(\mathcal{W}; \mathcal{W}^{\text{ref}}) \geq \Gamma_s, \quad i = 1, \dots, N_\theta, \quad (46b)$$

$$\text{tr}(\mathbf{R}_x(\mathcal{W})) \leq P_{\max}, \quad (46c)$$

which is a convex QCQP that can be readily solved by standard optimization tools.

In summary, starting from a feasible solution \mathcal{W}^{ref} , each iteration updates the auxiliary variables based on (39), constructs the MM minorants with (45), solves (46), and sets its optimizer as the new reference beamformers for the next iteration. The iterations terminate when the relative improvement of the true weighted sum rate falls below a prescribed tolerance. Since the WMMSE reformulation and MM minorants are tight at the current iterate, the algorithm preserves feasibility and monotonically improves the weighted sum rate. Following standard WMMSE/MM arguments [10], it converges to a stationary point of (35).

V. SIMULATION RESULTS

In this section, we evaluate the proposed MIMO-AFDM ISAC design in a high-mobility multiuser scenario. Unless otherwise specified, we set $N_t = N_r = 6$, $N = 64$,

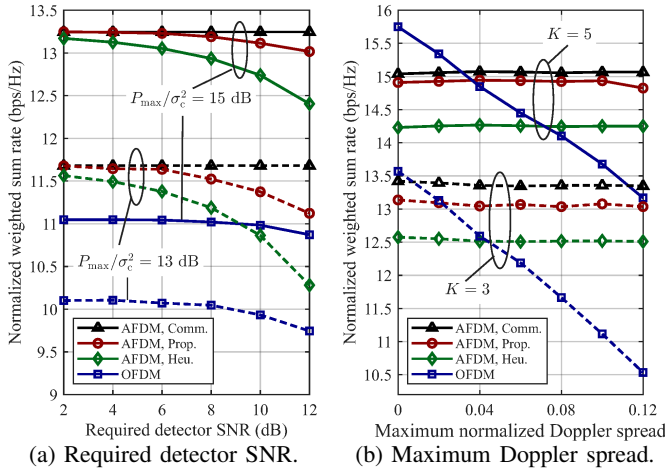


Fig. 1: Weighted sum rate under different settings.

$Q = 16$, $\ell_{\max} = 8$, $N_{\text{cpp}} = 10$, $P_{\max}/\sigma_c^2 = 15$ dB, and $\mu_k = 1$, $\forall k$. The $K = 3$ single-antenna users are located at $\{-45^\circ, -10^\circ, 20^\circ\}$. Each communication channel contains three delay-Doppler paths with gains distributed as $\mathcal{CN}(0, 1/3)$; their delays are drawn from $\{0, \dots, \ell_{\max}\}$, and their normalized Doppler shifts are uniformly distributed over $[-\nu_{\max}, \nu_{\max}]$ with $\nu_{\max} = 0.1$. The sensing sector is $\Theta_{\text{sen}} = [30^\circ, 50^\circ]$, with a target at $\theta_t = 40^\circ$. The chirp parameters are set as $c_1 = (2\nu_{\max} + 1)/(2N)$ and $c_2 = 1/(2N)$. We compare the proposed joint design, denoted by **AFDM, Prop.**, with three benchmarks: **OFDM**, which uses the same optimization framework with $c_1 = c_2 = 0$; **AFDM, Heu.**, which applies a sequential heuristic algorithm that first designs the sensing beams and then optimizes the communication beams; and **AFDM, Comm.**, which removes the sensing constraints and serves as a communication-only upper bound.

The rate-sensing tradeoff is shown in Fig. 1a. As the required detector SNR γ_{req} increases, stricter sensing requirements force more spatial resources to be steered toward the sensing sector, thereby reducing the weighted sum rate. The proposed AFDM scheme remains closest to the communication-only benchmark and consistently outperforms both OFDM and the heuristic AFDM design. The gain over OFDM demonstrates the robustness of AFDM against Doppler-induced dispersion, while the gain over the heuristic design highlights the benefits of jointly optimizing the communication and sensing beamformers. Fig. 1b evaluates the impact of the maximum normalized Doppler spread ν_{\max} . For small ν_{\max} , the channel is nearly quasi-static and OFDM remains competitive. As ν_{\max} increases, however, OFDM suffers from Doppler-induced inter-carrier interference, whereas AFDM achieves a higher rate by better matching the doubly dispersive channel. Consequently, the AFDM gain becomes more pronounced in the high-mobility regime.

Fig. 2 compares the normalized delay-Doppler detection maps. Although AFDM and OFDM satisfy the same target-illumination requirement, AFDM produces a more concentrated target peak with a lower sidelobe floor. In contrast, OFDM exhibits stronger Doppler-induced leakage, which

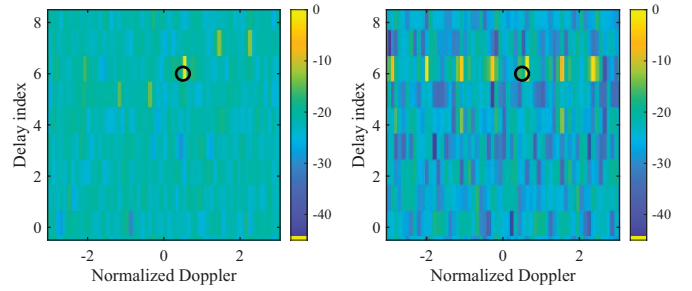


Fig. 2: Normalized delay-Doppler detection maps. (Target: black circle. Left: AFDM; right: OFDM).

raises the background level and makes the target less distinguishable. These results confirm that AFDM improves both the communication-sensing tradeoff and the reliability of data-aided delay-Doppler sensing in doubly dispersive channels.

VI. CONCLUSION

We have investigated sensing-constrained beamforming in the monostatic multiuser MIMO-AFDM ISAC downlink with doubly dispersive channels. By linking the expected matched-bin detector SNR to the transmit beamforming, we derived a detector-SNR-based sector-illumination constraint and solved the resulting weighted sum-rate maximization via a WMMSE-MM algorithm with convex QCP beamformer updates. Simulations confirmed the enhanced robustness of AFDM over OFDM in high-mobility doubly dispersive channels, motivating future extensions to more complex sensing scenarios.

REFERENCES

- [1] C. Sturm and W. Wiesbeck, "Waveform design and signal processing aspects for fusion of wireless communications and radar sensing," *Proc. IEEE*, vol. 99, no. 7, pp. 1236–1259, Jul. 2011.
- [2] F. Liu *et al.*, "Integrated sensing and communications: Toward dual-functional wireless networks for 6G and beyond," *IEEE J. Sel. Areas Commun.*, vol. 40, no. 6, pp. 1728–1767, Jun. 2022.
- [3] H. S. Rou, V. Savaux, Z. Sui, G. T. F. Abreu, and Z. Liu, "AFDM: Evolving OFDM towards 6G+," Feb. 2026. [Online]. Available: <https://arxiv.org/abs/2602.08163>
- [4] A. Bemani, N. Ksairi, and M. Kountouris, "Affine frequency division multiplexing for next generation wireless communications," *IEEE Trans. Wireless Commun.*, vol. 22, no. 11, pp. 8214–8229, Nov. 2023.
- [5] H. S. Rou *et al.*, "From orthogonal time-frequency space to affine frequency-division multiplexing: A comparative study of next-generation waveforms for integrated sensing and communications in doubly dispersive channels," *IEEE Signal Process. Mag.*, vol. 41, no. 5, pp. 71–86, Sep. 2024.
- [6] A. Bemani, N. Ksairi, and M. Kountouris, "Integrated sensing and communications with affine frequency division multiplexing," *IEEE Wireless Commun. Lett.*, vol. 13, no. 5, pp. 1255–1259, May 2024.
- [7] Y. Ni, P. Yuan, Q. Huang, F. Liu, and Z. Wang, "An integrated sensing and communications system based on affine frequency division multiplexing," *IEEE Trans. Wireless Commun.*, vol. 24, no. 5, pp. 3763–3779, May 2025.
- [8] F. Zhang *et al.*, "AFDM-enabled integrated sensing and communication: Theoretical framework and pilot design," *IEEE J. Sel. Areas Commun.*, vol. 44, pp. 310–324, 2026.
- [9] J. Qian, Y. Liang, Y. Zou, X. Song, and Y. Huang, "The transmit design for ISAC system based on affine frequency-division multiplexing," *IEEE Trans. Instrum. Meas.*, vol. 75, Art. no. 6502711, 2026.
- [10] Q. Shi, M. Razaviyayn, Z. -Q. Luo, and C. He, "An iteratively weighted MMSE approach to distributed sum-utility maximization for a MIMO interfering broadcast channel," *IEEE Trans. Signal Process.*, vol. 59, no. 9, pp. 4331–4340, Sep. 2011.